A Nuclear Localization Sequence Endows Human Pancreatic Ribonuclease with Cytotoxic Activity†

Montserrat Bosch,‡ Antoni Benito,‡ Marc Ribó,‡ Teresa Puig,‡ Bruno Beaumelle,§ and Maria Vilanova*,‡

Laboratori d'Enginyeria de Proteïnes, Departament de Biologia, Facultat de Ciències, Universitat de Girona, Campus de Montilivi s/n, E-17071 Girona, Spain, and UMR 5539 CNRS, Departmente Biologie-Santé, Université Montpellier II, 34095 Montpellier Cedex 05, France

Received September 24, 2003; Revised Manuscript Received December 29, 2003

ABSTRACT: Some members of the ribonuclease superfamily, such as Onconase, are cytotoxic to cancer cells. This is not the case for human pancreatic ribonuclease. This lack of cytotoxicity is probably a result of the inhibition exerted by the cytosolic ribonuclease inhibitor once the protein has reached the cytosol. Until now, all cytotoxic human pancreatic ribonuclease variants have been described as being resistant to the inhibitor. Here, we report on the characterization of a cytotoxic variant of human pancreatic ribonuclease which has an Arg triplet introduced onto one of its surface-exposed loops. Despite its sensitivity to the inhibitor, this variant, called PE5, was only 5−15 times less cytotoxic than Onconase. When it was taken up by cells, it was only observed within late compartments of the endocytic pathway, probably because the number of molecules transported to the cytosol was too small to allow their visualization. Nuclear import assays showed that the Arg triplet endows PE5 with a nuclear localization signal. In these experiments, PE5 was efficiently transported to the nucleus where it was initially localized in the nucleolus. Although the Arg introduction modified the net charge of the protein and somehow impaired recognition by the cytosolic inhibitor, control variants, which had the same number of charges or were not recognized by the inhibitor, were not toxic. We concluded that targeting a ribonuclease to the nucleus results in cytotoxicity. This effect is probably due to ribonuclease interference with rRNA processing and ribosome assembly within the nucleolus.

Members of the pancreatic ribonuclease superfamily display an array of biological activities ranging from cytotoxicity to angiogenesis. Among them, cytotoxicity is one of the most attractive since such enzymes could be used, alone or conjugated to ligands or antibodies, as therapeutic agents for cancer treatment (for a review, see ref *1*). Onconase is a monomeric ribonuclease isolated from *Rana pipiens* (northern leopard frog) and is selectively toxic to cancer cells both *in vitro* and *in vivo* (*2*). It nevertheless shows renal toxicity at high concentrations (*3*). Generating a cytotoxic variant of a human ribonuclease such as the human pancreatic ribonuclease (HP-RNase)[1] would undoubtedly provide a potentially useful therapeutic agent which would be expected to have low immunogenicity and renal toxicity.

Despite the fact that Onconase is currently in phase III of human clinical trials (*2*), the molecular basis underlying the cytotoxicity of Onconase or other cytotoxic ribonucleases is not well understood.

It is suggested that cytotoxic ribonucleases first interact with the surface of the target cell, before endocytosis. At some as yet unidentified stage of the endo/exocytic pathway (*4*), the ribonucleases are then translocated to the cytosol. Once there, they have to either evade or titrate the cytosolic ribonuclease inhibitor (RI) to degrade RNA and kill the cell (*5*).

A number of features appear to be necessary for a ribonuclease to be cytotoxic. First, the protein should be stable at physiological temperature (*5*). Indeed, Onconase is a highly temperature-stable molecule (*6*), and increasing stability has been shown to enhance toxicity (*7*, *8*).

Second, endocytosis efficiency can also dramatically affect ribonuclease cytotoxicity. For instance, monomers of RNase A or HP-RNase, chemically conjugated or fused to ligands such as transferrin, growth factors, or antibodies, are more

† This work was supported by grants from the Ministerio de Ciencia y Tecnologia (BMC2000-0138-CO2-02), from the Generalitat de Catalunya (SGR2000-64 and SGR2001-00196), and from a Picasso French-Spanish exchange program (HF2001-0017). M.B. gratefully acknowledges a predoctoral fellowship from CIRIT, Generalitat de Catalunya. We are also indebted to the Fundació "M. F. de Roviralta" (Barcelona, Spain) for equipment purchasing grants.

* To whom correspondence should be addressed. Fax: +34-972-418173. E-mail: maria.vilanova@udg.es.

‡ Universitat de Girona.

§ Université Montpellier II.

[1] Abbreviations: BSA, bovine serum albumin; BS-RNase, bovine seminal ribonuclease; C>p, cytidine 2′,3′-cyclic monophosphate; DMEM, Dulbecco's modified Eagle's medium; DTT, dithiothreitol; EGF, epidermal growth factor; FCS, fetal calf serum; FRET ArUAA, 6-carboxyfluorescein−dArUdAdA−6-carboxytetramethylrhodamine; HP-RNase, human pancreatic ribonuclease; HPLC, high-performance liquid chromatography; IC_{50}, RNase concentration required to inhibit by 50% cell protein synthesis; Lamp, lysosome-associated membrane protein; LB, Luria-Bertani medium; mAb, monoclonal antibody; MALDI-TOF, matrix-assisted laser desorption ionization time-of-flight; NLS, nuclear localization signal; PBS, phosphate-buffered saline; PCR, polymerase chain reaction; poly(C), poly(cytidylic acid); RI, human ribonuclease inhibitor; RNase A, bovine pancreatic ribonuclease; TFA, trifluoroacetic acid; TCA, trichloroacetic acid; $T_{1/2}$, midpoint of the thermal denaturation curve.

10.1021/bi035729+ CCC: $27.50
Published on Web 02/04/2004

avidly taken up by the target cells and, consequently, become much more cytotoxic (*1*).

Third, the ribonuclease needs to avoid inhibition by the RI (*5*). The RI is thought to act as a safeguard against secreted ribonucleases that may inadvertantly appear in the cytoplasm (*9*). It binds to pancreatic-type ribonucleases with a 1:1 stoichiometry and has a dissociation constant (K_i) in the picomolar range (*8*, *10*). In contrast, the affinity of the RI for Onconase is 1000-fold lower, and Onconase is thought not to be inhibited by the RI (*11*). Moreover, when ribonucleases were engineered by site-directed mutagenesis to impair their binding to the RI, cytotoxic mutants were obtained (*8*, *10*, *12*, *13*). Hence, converting an innocuous ribonuclease into a cytotoxic one seems to require resistance to the inhibitor.

Because the RI is present in the cytosol but not in the nucleus (*14*), transporting any ribonuclease into the nucleus by the nuclear import machinery would overcome the inhibitor action. There is, in fact, one member of the ribonuclease family, angiogenin, which is RI-sensitive, and which is directed into the nucleus. Nevertheless, angiogenin is not cytotoxic. This is probably due to its very weak catalytic activity which is 10^5-10^6 times lower than that of RNase A (*15*). Its angiogenic function nevertheless requires this weak ribonuclease activity as well as its nucleolar localization. However, it is not clear how angiogenin enhances rRNA production and how this is linked to its main function in the nucleus, which is assumed to be gene expression modulation during angiogenesis (*16*, *17*).

In this study, we constructed a set of HP-RNase variants designed to evade the RI and/or to interact with the cell membrane, by introducing mutations within the three surface-exposed loops involved in RI binding. These amino acid changes included the introduction of an integrin-targeting sequence (i.e., an RGD motif) (*18*), as well as other changes aimed at reducing the level of RI−ribonuclease interaction. Surprisingly, the most cytotoxic variant, PE5, is RI-sensitive. Its cytotoxicity can be explained by the presence of a nuclear localization signal (NLS) within its structure. Nuclear targeting probably enabled this ribonuclease to interact with rRNA before it is packaged within ribosomes. This is a new way of obtaining cytotoxic ribonuclease variants: targeting them to a site within the cell, which is free of the cytosolic inhibitor.

MATERIALS AND METHODS

Materials. Escherichia coli strain BL21(DE3), plasmid pET17b, and ribonuclease substrate 6-carboxyfluorescein−dArUdAdA−6-carboxytetramethylrhodamine (FRET ArU-AA) were supplied by Novagen. Oligonucleotides used for site-directed mutagenesis, molecular biology enzymes, Pronase, and ribosomal RNA (rRNA; 16S and 23S) were supplied by Roche. The human ribonuclease inhibitor was purchased from Promega and fluorescein-labeled epidermal growth factor (EGF) from Molecular Probes. Other chemicals were supplied by Sigma. Radiochemicals were supplied by ICN Biomedicals. Fluorescein-labeled BSA conjugated with SV40 NLS (fluorescein−BSA−NLS) was kindly provided by U. Greber (University of Zurich, Zurich, Switzerland). Cell lines were supplied by American Type Culture Collection (Manassas, VA). Dulbecco's modified Eagle's medium (DMEM) and fetal calf serum (FCS) were supplied by Invitrogen.

Table 1: Localization of the Substitutions within the Primary and Secondary Structure of HP-RNase Variants Generated for This Study

variant	α2 and loop α2β1	loop β2β3	loop β4β5
PE5	−	−	G89R, S90R
PE3	R31E	−	R91A
PE3I1	R31E, Q37R, R39D	−	R91A
PE3I2	R31E	K66R, N67G, G68D	R91A
PI5	Q37R, R39D	K66R, N67G, G68D	G89R, S90G, R91D

Construction of HP-RNase Variants. HP-RNase variants were constructed by site-directed mutagenesis following a strategy described elsewhere (*19*). PM9 is the wild-type HP-RNase that was used to generate PM5, in which the 20 residues of its N-terminus are substituted with the corresponding sequence from BS-RNase, although in fact only five of these residues differ from the HP-RNase sequence. We used this PM5 variant as a template to prepare the other mutants, because it exhibited a higher thermostability than wild-type HP-RNase (*20*). The oligonucleotides used for introducing mutations were 27−30 residues long. PCR products, corresponding to the whole mutated genes, were digested with *Sal*I and *Nde*I and inserted into pET17b. Screening was performed by restriction analysis and confirmed by sequence determination. The various HP-RNase mutants that were generated for this study are presented in Table 1.

Protein Expression and Purification. Transfected BL21-(DE3) cells were grown until an OD_{550} of 1.5 was reached. Protein expression was induced by adding isopropyl thiogalactoside to a final concentration of 1 mM. After 3−4 h, the cells were collected by centrifugation and lysed with a French press, and inclusion bodies were harvested by centrifugation. HP-RNase purification has been described elsewhere (*20*). Briefly, inclusion bodies were solubilized and reduced, and the protein was refolded by drop dilution into Tris buffer containing L-arginine (0.5 M), EDTA (2 mM), and oxidized glutathione (1 mM). After concentration and dialysis, the sample was purified on a MonoS HR 5/5 FPLC column (Amersham Biosciences). A yield of 5−20 mg of protein per liter of culture was obtained, depending on the variant.

The Onconase gene, a generous gift from R. T. Raines (University of Wisconsin, Madison, WI), was expressed and then Onconase purified using the same method described in the previous paragraph. The recombinant enzyme was activated by removing the N-terminal Met residue with *Aeromonas* aminopeptidase before cyclization of the N-terminal Gln. To analyze the homogeneity of purified HP-RNase variants, each sample was subjected to reversed-phase HPLC on a 214TP Vydac C-4 column. A linear gradient was generated from 0.1% TFA to 100% acetonitrile in 0.1% TFA. The molecular mass of each variant was confirmed by MALDI-TOF mass spectrometry using Bruker-Biflex equipment in the Biocomputation and Protein Sequencing Facility of the Institut de Biotecnologia i Biomedicina at the Universitat Autònoma de Barcelona (Barcelona, Spain).

The protein concentration of each variant was determined by UV spectroscopy using an extinction coefficient ϵ_{278} of

Table 2: Biochemical Characterization of the HP-RNase Variants

variant	$T_{1/2}$ (°C)[a]	$(k_{cat}/K_m)_{rel}$[b] for C>p (%)	$(V_{max}/[E_0]K_m)_{rel}$[b] for poly(C) (%)	K_i[c] (nM)	net[d] charge
PE5	45.7	93.3	61.4	ND[e]	+6
PE3I1	52.0	77.0	71.0	0.8 ± 0.13	0
PE3I2	46.9	82.0	51.7	0.77 ± 0.14	0
PE3	53.1	70.6	78.0	0.42 ± 0.09	+1
PI5	40.5	64.2	53.7	1.34 ± 0.17	+1
PM5	58.3	100	100	ND[e]	+4
PM9	53.7	107.2	130.0	ND[e]	+6

[a] Thermal denaturation experiments monitored by fourth-derivative absorption spectroscopy were used to calculate the temperature at the midpoint of the thermal transition ($T_{1/2}$). [b] Efficiency of cleavage of the indicated RNA substrate. Values obtained for PM5 were set to 100%. [c] Values of K_i (±standard error) for the HP-RNase variants are for inhibition by the RI of FRET ArUAA cleavage at pH 6.0 and 25 °C. [d] Expressed as the difference between Arg with Lys and Asp with Glu. [e] Not determined, due to the high affinity of the RI for these variants.

8200 M^{-1} cm^{-1}, calculated using the method devised by Gill and von Hippel (*21*). The extinction coefficient for Onconase (ϵ_{278}) equaled 10 280 M^{-1} cm^{-1} (*10*).

Ribonuclease Inhibitor Binding Assay. Fifteen nanograms of each ribonuclease in 20 μL of 125 mM NaCl, 10 mM DTT, 1 mM EDTA, and 20 mM Hepes (pH 7.0) received either 0 or 40 units of the RI (where 1 unit is the amount of the RI required to inhibit the activity of 5 ng of RNase A by 50%). After 10 min at 37 °C, 4 μg of 16 S and 23S rRNA were added to each sample and the samples were incubated for a further 10 min at 37 °C. Reactions were stopped by the addition of a loading buffer [40% (w/v) sucrose, 0.2% (v/v) diethyl pyrocarbonate, and 0.25% (w/v) bromophenol blue] and the mixtures subjected to electrophoresis in an agarose gel [1.2% (w/v)] containing ethidium bromide.

K_i Calculation. The K_i values for HP-RNase variants were determined by assessing the cleavage of the FRET ArUAA substrate in the presence of increasing concentrations of the RI (*10*). K_i values were calculated by fitting the steady-state rates to an equation that describes inhibition by tight-binding inhibitors (*22*). The ribonuclease concentration was kept below the K_i value.

Determination of Steady-State Kinetic Parameters. Spectrophotometric assays (*23*) were used to determine the kinetic parameters for the cleavage of poly(C) and the hydrolysis of C>p by HP-RNase variants. For C>p, the concentration of the enzyme was 0.1 μM, the initial concentration of C>p ranged from 0.1 to 5.5 mM, and the activity was measured by recording the increase in absorbance at 296 nm. For assays with poly(C), the enzyme concentration was 5 nM, the initial concentration of the substrate ranged from 0.1 to 2.5 mg/mL, and the decrease in absorbance at 294 nm was monitored. Assays were carried out at 25 °C in 0.2 M sodium acetate buffer (pH 5.5) using quartz cells with path lengths of 1 and 0.2 cm for C>p and poly(C), respectively. Steady-state kinetic parameters were obtained by nonlinear regression analysis using the program ENZFITTER (*24*). The values presented in Table 2 are the average of three determinations.

Thermal Denaturation Experiments. The absorption spectra of the enzymes [1 mg/mL in 50 mM sodium acetate (pH 5.0)] were recorded between 250 and 310 nm at different temperatures using a Perkin-Elmer spectrometer with a thermostated cell holder. The temperature was increased from 20 to 80 °C in 2−3 °C steps, and the $T_{1/2}$ value of each variant was determined as previously described (*25*). Standard errors for the $T_{1/2}$ were less than 1%.

Circular Dichroism. A Jasco-J810 spectropolarimeter equipped with a temperature-regulated sample chamber was used. The proteins [0.25 mg/mL in 10 mM Tris (pH 7.3)] were filtered using 0.2 μm filters and placed in a quartz cell with an optical path length of 0.1 cm. The sample compartment and solution were purged with dry nitrogen before CD spectra were recorded (185−250 nm) at 37 °C using a scan speed of 20 nm/min, a bandwidth of 1 nm, and a time response of 1 s. The spectra were signal-averaged over four scans.

Protease Digestion Experiments. Ribonucleases (13 μg) in 14 mM $CaCl_2$ and 10 mM Tris-HCl (pH 7.3) were treated with thermolysin (from 1.4 ng to 1.4 μg) for 30 min at 43 °C. Digestions were stopped by adding 20 mM EGTA, and samples were resolved by SDS−PAGE (using tricine gels with 12.5% acrylamide) before gel staining with Coomassie blue. For quantification, duplicate gels were scanned and bands were quantified using ImageQuant (Amersham Biosciences).

Protein Labeling. Transferrin was conjugated to Cy5 using a commercial kit (Amersham Biosciences). Ribonuclease labeling with ^{125}I was performed using the Iodogen reagent (*26*). A Cys was introduced by PCR (*19*) at the carboxyl terminus of PM5 and PE5 to allow fluorochrome conjugation. PM5cys and PE5cys were reacted with Alexa Fluor 594 C5 maleimide (Molecular Probes) essentially as recommended by the manufacturer. Briefly, a 10-fold molar excess of DTT was first added to the RNase to reduce the carboxyl-terminal cysteine. After 20 min, DTT was removed by gel filtration on a Sephadex G-25 column. A 20-fold molar excess of reactive dye (20 mM in PBS) was immediately added to the protein. The reaction was stopped after 2 h by adding 1 mM reduced glutathione. The conjugates were then concentrated at 4 °C (Centricon-plus, Millipore), dialyzed extensively against PBS, filter-sterilized, and stored at −20 °C. The maleimide reaction on the Cys generates a thioether bond which is considered to be irreversible within animal cells. These Alexa Fluor 594 conjugates are efficiently excited by the 568 nm spectral line of the confocal Ar−Kr laser.

Assessment of Ribonuclease Uptake. K562 cells (10^7 cells/mL) were incubated for different lengths of time in DMEM and BSA containing ^{125}I-labeled ribonuclease (~0.2 μM). Nonbound ligand was then removed by three washes in ice-cold PBS. Cells were resuspended in Pronase (0.3% in PBS), left for 45 min on ice, and then spun at 21000*g* for 3 min through a cushion of dibutyl phthalate. Internalization was calculated as the fraction of cell-associated label becoming resistant to Pronase scraping (*26*).

Cytotoxicity Assays. Cells were grown in DMEM supplemented with 10% FCS, 50 units/mL penicillin, and 50 μg/mL streptomycin. The cytotoxicity of HP-RNase variants was assayed on five human cell lines [K-562 (chronic myelogenous leukemia), A-431 (epidermoid carcinoma), MCF-7 (breast carcinoma), Daudi (Burkitt's lymphoma), and HeLa cells (cervix carcinoma)] which were seeded into 96-well plates at the appropriate density, i.e., 7500 (for MCF-7), 2500 (for A431, HeLa, and Daudi), and 1250 (for K562) cells per well. After 3 days, [^{35}S]Met (500 000 cpm per well) was

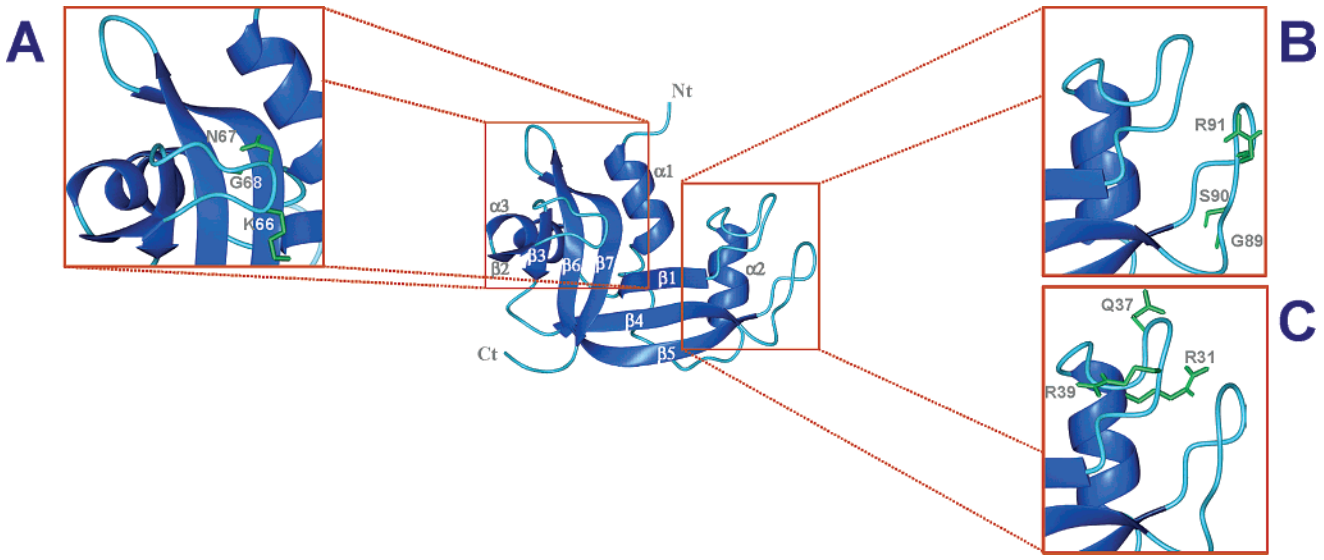

FIGURE 1: Ribbon representation of the three-dimensional structure of HP-RNase showing the location of the substituted residues: (A) loop $\beta2\beta3$, (B) helix $\alpha2$ and loop $\alpha2\beta1$, and (C) loop $\beta4\beta5$. Substituted amino acid side chains are shown in green. The substitutions characterizing each HP-RNase variant are depicted in Table 1. This figure was drawn with MOLMOL (*42*).

added for 24 h. The medium was then removed (after plate centrifugation in the case of the K562 and Daudi cells); the cells were then lysed with NaOH, and proteins were precipitated with 15% TCA. Proteins were collected onto glass fiber filters using a cell harvester and washed with 5% TCA, and the filter radioactivity was counted using a liquid scintillation counter. Background incorporation was obtained from cells treated with 1 mM cycloheximide (*27*). The results for a single experiment were the average of four determinations, and the experiments were repeated three times. The IC_{50} values represent the concentration of the ribonuclease required to inhibit cell protein synthesis by 50%.

Confocal Immunofluorescence Microscopy. A431 cells were seeded onto 12 mm diameter coverslips in 24-well plates (5×10^4 cells/well) the day before the experiment. They were labeled with the fluorescent ribonuclease (~350 nM) for 24 h in DMEM supplemented with 5% FCS, and 100 nM Cy5-labeled transferrin for the last 45 min. When indicated, 100 ng/mL fluorescein-labeled EGF was present for the last hour of labeling. Cells were then fixed for 15 min at room temperature in PBS containing 3.7% paraformaldehyde, left for 15 min in PBS containing 50 mM NH_4Cl and for 10 min in PBS containing 1 mg/mL BSA, permeabilized in PBS supplemented with 1 mg/mL BSA and 0.05% saponin, and then treated with antibodies diluted in permeabilization buffer. The human mannose 6-phosphate receptor (M6PR) was revealed using a chicken antibody kindly provided by H. Rochefort (INSERM, Montpellier, France) and fluorescein-labeled rabbit anti-chicken antibodies (Nordic). Anti-lamp (lysosomal-associated membrane protein) 1 and 2 monoclonal antibodies (mAbs) were supplied by the Iowa Developmental Studies Hybridoma Bank, and anti-BIP (binding protein, a major chaperone of the endoplasmic reticulum) mAb was supplied by Transduction Laboratories. These antibodies were revealed using fluorescein-conjugated goat anti-mouse antibodies (Sigma). Sheep antibodies against human TGN46 (a marker for the *trans*-Golgi network) (Serotec) were detected using fluorescein-labeled donkey anti-sheep antibodies (Nordic). Finally, cells were mounted in 100 mM Tris-HCl (pH 8.5) containing 25% (v/v) glycerol, 10% Mowiol, and 0.5 M 1,4-diazabicyclo[2.2.2]octane and examined under a Leica confocal microscope using a lens with a magnification of 63×. Bleed-through from one channel to the other was negligible. Medial optical sections were recorded.

Nuclear Import Assays. Cytosol (~3 mg/mL) was purified from HeLa S3 cells as described elsewhere (*28*) and stored at −80 °C. Import reactions were performed at 30 °C for 0−20 min using digitonin-permeabilized HeLa cells (*29*), cytosol, and, as indicated, 2.3 μM fluorescent substrate Alexa Fluor 594 ribonuclease, 10 μM fluorescein−BSA−NLS, an ATP regenerating system (1 mM ATP, 5 mM phosphocreatine, and 20 units/mL creatine phosphokinase), an ATP depleting system (100 units/mL apyrase), 0.025% CHAPS, or 300 μM GTPγS (*16*). Cells were then washed and fixed with 3.7% paraformaldehyde. When indicated, the nucleus was stained with 100 nM Sytox green (Molecular Probes) in PBS for 15 min before washing and mounting were carried out.

For immunofluorescence localization of Ki-67, following the import reaction and fixation, cells were permeabilized in PBS containing 0.1% Triton X-100 for 2 min at 4 °C (*30*) and incubated with a mouse monoclonal antibody anti-Ki67 (Dako) and then with fluorescein-labeled goat anti-mouse antibodies. Cells were then mounted for confocal microscopic examination as described above.

RESULTS

Design and Production of HP-RNase Variants. The three-dimensional structure of an HP-RNase variant has been determined (*31*), and a complex between this enzyme and the RI has been modeled by superimposing the atomic coordinates of this variant onto those of RNase A in its complex with the RI (*32*). From this model, it appears that three surface-exposed loops of HP-RNase, $\alpha2\beta1$ (residues 30−42), $\beta2\beta3$ (residues 64−71), and $\beta4\beta5$ (residues 87−96) significantly contribute to the contacts between both proteins. The structural location of these loops is presented in Figure 1. With the aim of preparing cytotoxic variants,

we reasoned that these three loops would be suitable locations for introducing mutations that could prevent RI binding.

In the PE3 variant, two basic residues were altered at positions 31 (α-helix 2) and 91 (*β*4−*β*5 loop). At position 31, Arg was replaced with an acidic residue to promote electrostatic repulsion with two RI acidic residues: Asp36 and Glu13. At position 91, a residue with a short side chain was chosen to suppress a large number of van der Waals contacts between both proteins. Two Arg residues were introduced before Arg91 in the third loop to generate the PE5 variant. The introduction of these two bulky basic residues in the PE5 variant was thought to be likely to promote steric hindrance in the RI−HP-RNase complex.

A second group of mutants bears an RGD motif (*18*) which was chosen so that their interaction with the cell membrane would be favored and, possibly, so that HP-RNase internalization would be enhanced. This tripeptide has been shown to promote cell binding when inserted into a protein (*33*), and has been used to target tumor cells *in vivo* (*34*). In an attempt to simultaneously weaken the interaction with the RI, we introduced the RGD motif within loops that bind the RI. Specifically, the RGD motif replaced residues 37−39 (α2*β*1 loop), 66−68 (*β*2*β*3 loop) and/or 89−91 (*β*4*β*5 loop). Three RGD variants were produced. PE3I1 and PE3I2 bear this motif within the first and second loops, respectively, whereas in PI5, all three loops have an RGD motif. Variants PE3I1 and PE3I2 also carry additional R31E and R91A mutations aimed at diminishing the strength of the ribonuclease−RI interaction. The variants are presented in Table 1. They were produced and purified from *E. coli* inclusion bodies (*20*). In addition, the location of the amino acid changes in the three-dimensional structure of the HP-RNase variant (*31*) is presented in Figure 1.

Stability of HP-RNase Variants. To be cytotoxic, either in cell culture or *in vivo*, a ribonuclease should retain its native conformation at physiological temperatures (*7*). Different experiments were performed to evaluate whether the residue substitutions had altered the stability of the selected variants. The variants showed overlapping CD spectra (data not shown), indicating that the secondary structure of the protein was not affected by the mutations. Thermal denaturation experiments were then used to calculate the temperature at the midpoint of the thermal transition ($T_{1/2}$). All the substitutions produced a decrease in the thermal stability of the variants, with PE3I2, PE5, and PI5 being affected the most (Table 2). These findings were confirmed when susceptibility to proteolysis was examined. Thermolysin digestion experiments indicated that the order of conformational flexibility is as follows: PM5 < PM9 < PE5 < PI5 (data not shown).

All HP-RNase Variants Retain Catalytic Activity. It was also important to check that the mutations did not suppress the ribonuclease activity. To this end, steady-state kinetic parameters were determined for the hydrolysis of C>p, and for the cleavage of poly(C). Whatever the assay and compared to the parent molecule, PM5, all the variants retain a catalytic efficiency between 50 and 93% (Table 2). Hence, the mutations did not drastically affect HP-RNase catalytic activity.

Interaction of the HP-RNase Variants with the RI. RI avoidance is assumed to be a prerequisite for obtaining a cytotoxic HP-RNase mutant (*8*). The interaction of the RI with the different variants was first analyzed qualitatively by monitoring the cleavage of rRNA by each variant in the absence or presence of RI (Figure 2). Wild-type HP-RNase was inhibited by the RI, while Onconase was insensitive to it. Under the assay conditions, all variants remained active to some extent in the presence of the RI (Figure 2), although PE5 only weakly evaded the RI in the test tube. A quantitative measure of the interaction with the inhibitor was then performed by assessing the cleavage of FRET ArUAA in the presence of increasing RI concentrations. Using the FRET assay, an enzyme concentration below the value of K_i is required to determine the inhibition constant (*22*, *35*). The tight binding of the RI to PM5 and PE5 prevented the K_i measurements because of the low concentration of the free enzyme. The K_i values obtained for the other, less inhibitor-sensitive variants were within the nanomolar range (Table 2), as previously reported for other cytotoxic HP-RNase variants (*8*).

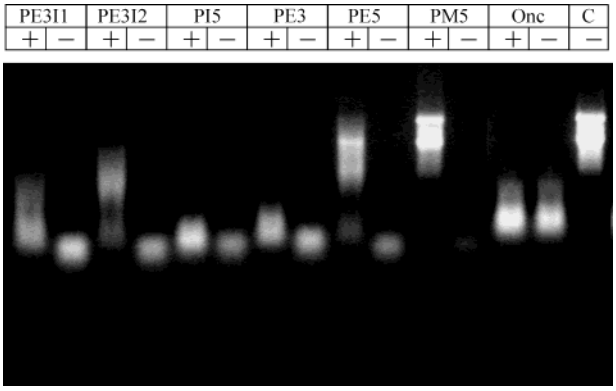

FIGURE 2: Inhibition of ribonucleolytic activity by the RI. Inhibition was assessed by visualizing on an agarose gel the ribonuclease-catalyzed degradation of 16S and 23S rRNA in the absence (−) and presence (+) of 40 units of the RI. C is the control assay without the ribonuclease enzyme. Onc represents Onconase. HP-RNase variants are described in Table 1. PM5 can be considered equivalent to wild-type HP-RNase (see the text for details). The intensity and the position of the rRNA bands correlate with the degree of ribonucleolytic activity. As ribonucleolytic activity in the assay decreases, both band intensities and apparent molecular masses increase.

Cytotoxicity. Variant toxicity was assessed on K562 and A431 cell lines (Figure 3A). As reported previously (*10*), Onconase displayed an IC_{50} value of 0.5 μM for K562 cells. At the maximum ribonuclease concentration used in the assay (30 μM), PM5, PE3I1, PE3I2, and PI5 did not affect the viability of either A431 or K562 cells. Despite being able to avoid RI, PE3 was only moderately cytotoxic, with an IC_{50} of >3 μM for all cell lines (Figure 3B). Surprisingly, and despite being only weakly resistant to the RI (Figure 2), PE5 was 10-fold more cytotoxic than PE3 (except in the case of K562). Indeed, PE5 was the most toxic variant, with an IC_{50} ranging from 0.3 to 3 μM (Figure 3B). These values are only 5−15 times higher than those observed for Onconase (Figure 3B). Hence, PE5 displays cytotoxicity on the same order of magnitude as those described for other cytotoxic HP-RNase variants (*8*, *12*).

All HP-RNase Variants Are Poorly Endocytosed. We then focused on the most cytotoxic variant, PE5, and first wondered whether enhanced endocytosis efficiency was responsible for its toxicity. We monitored the internalization rate of ^{125}I-labeled variants using K562 cells over the course

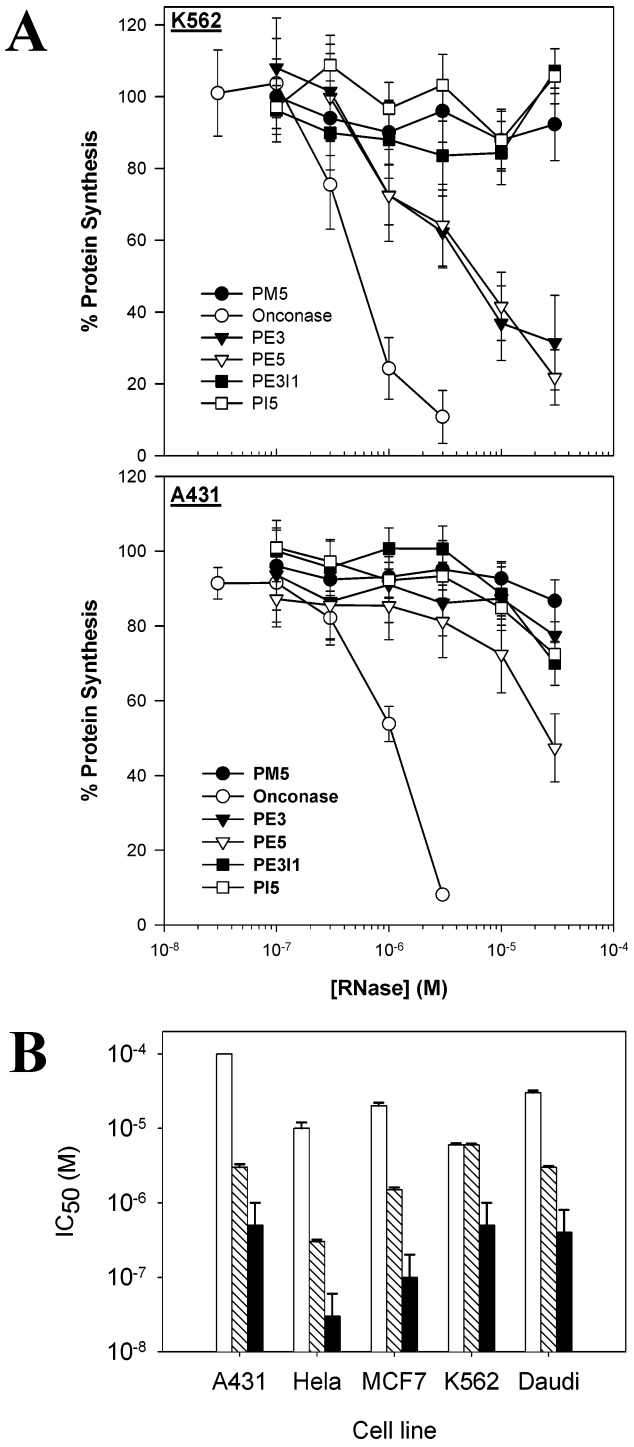

FIGURE 3: Cytotoxicity of ribonuclease variants. Cell viability was measured by monitoring the incorporation of [^{35}S]methionine into the newly synthesized protein after a 96 h incubation with a ribonuclease. Averages of three experiments are shown: (A) toxicity to A431 and K562 cell lines and (B) IC_{50} values for Onconase (black bars), PE5 (cross-hatched bars), and PE3 (white bars) for the indicated cell lines.

of 7 h (Figure 4). Under these conditions, Onconase was the only ribonuclease tested which was significantly internalized with 40% of [^{125}I]Onconase found inside the cell after 7 h. Hence, it seems likely that efficient Onconase internalization participates in its cytotoxicity. No significant internalization was observed using this assay for any of the HP-RNase variants (Figure 4 shows the results for PM5, PI5, and PE5; data not shown for the others). We concluded from

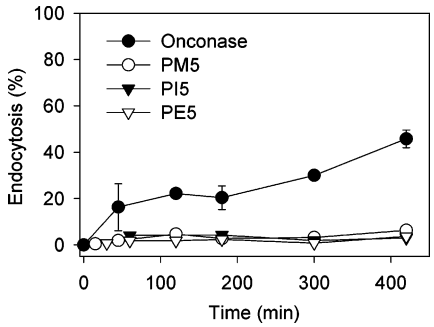

FIGURE 4: Internalization of radiolabeled ribonucleases by K562 cells. Cells were allowed to internalize the indicated ^{125}I-labeled ribonuclease at 37 °C. Internalization was calculated as the fraction of cell-associated label that is resistant to Pronase scraping.

the PI5 results that introduction of an RGD sequence, at least in the positions we selected, did not allow HP-RNase to be more efficiently taken up by cells. The cytotoxic variant PE5 was not internalized by K562 cells more efficiently than nontoxic variants, such as PM5. Hence, PE5 cytotoxicity was not the result of enhanced endocytosis efficiency.

Compared to its parent molecule (PM5), PE5 carries two additional positive charges. It has been shown that increasing the net charge of RNase A, albeit by 6 at least, enhanced its uptake and toxicity (*36*). Nevertheless, PM9, the wild-type protein, carries the same net charge as PE5 (see Table 2), and it is not cytotoxic (*8*). Hence, the net charge of PE5 does not explain its toxicity either.

PE5 Intracellular Routing. We then wondered whether PE5 cytotoxicity might be the result of a specific intracellular pathway. To follow the cytotoxic (PE5) and control (PM5) variants within cells, we added a Cys to their carboxyl termini so that they could be directly labeled with a bright fluorochrome through a stable thioether bond. In agreement with data obtained using [^{125}I]ribonucleases, these fluorescent conjugates could not be readily visualized within cells before they had been labeled for 24 h. At that time, they exhibited an identical intracellular localization. They were found in lysosomes, together with other tracers directed to this structure such as fluorescein-labeled EGF (Figure 5). They accumulated in structures which were efficiently labeled with antibodies against the major lysosomal membrane proteins Lamp-1 and Lamp-2, which are concentrated within lysosomes. The fluorescent ribonucleases were not observed within early endosomes (identified using fluorescent transferrin) or in late endosomes (identified using antibodies against the M6PR). They were also not found within the ER and *trans*-Golgi network labeled with anti-BIP and anti-TGN46 antibodies, respectively (Figure 5). We concluded that PE5 (Figure 5) and PM5 (not shown) are directed to lysosomes, where they accumulate. Hence, PE5 is not specifically sorted from PM5 within the endocytic network, and follows the default pathway to the lysosomes (*37*). However, a fraction of the molecules may translocate to the cytosol, likely before reaching the late elements of this route.

PE5 Is Targeted to the Nucleus. Alternatively, the cytotoxicity of PE5 could be explained by specific targeting, after cytosolic delivery, to a compartment rich in substrate but lacking the RI, i.e., the nucleus. Indeed, a pre-existing Arg triplet (residues 31−33; see Figure 1) is exposed in the parent PM5 molecule, and in PE5, an additional Arg triplet has been introduced in the facing loop (residues 89−91). We hypoth-

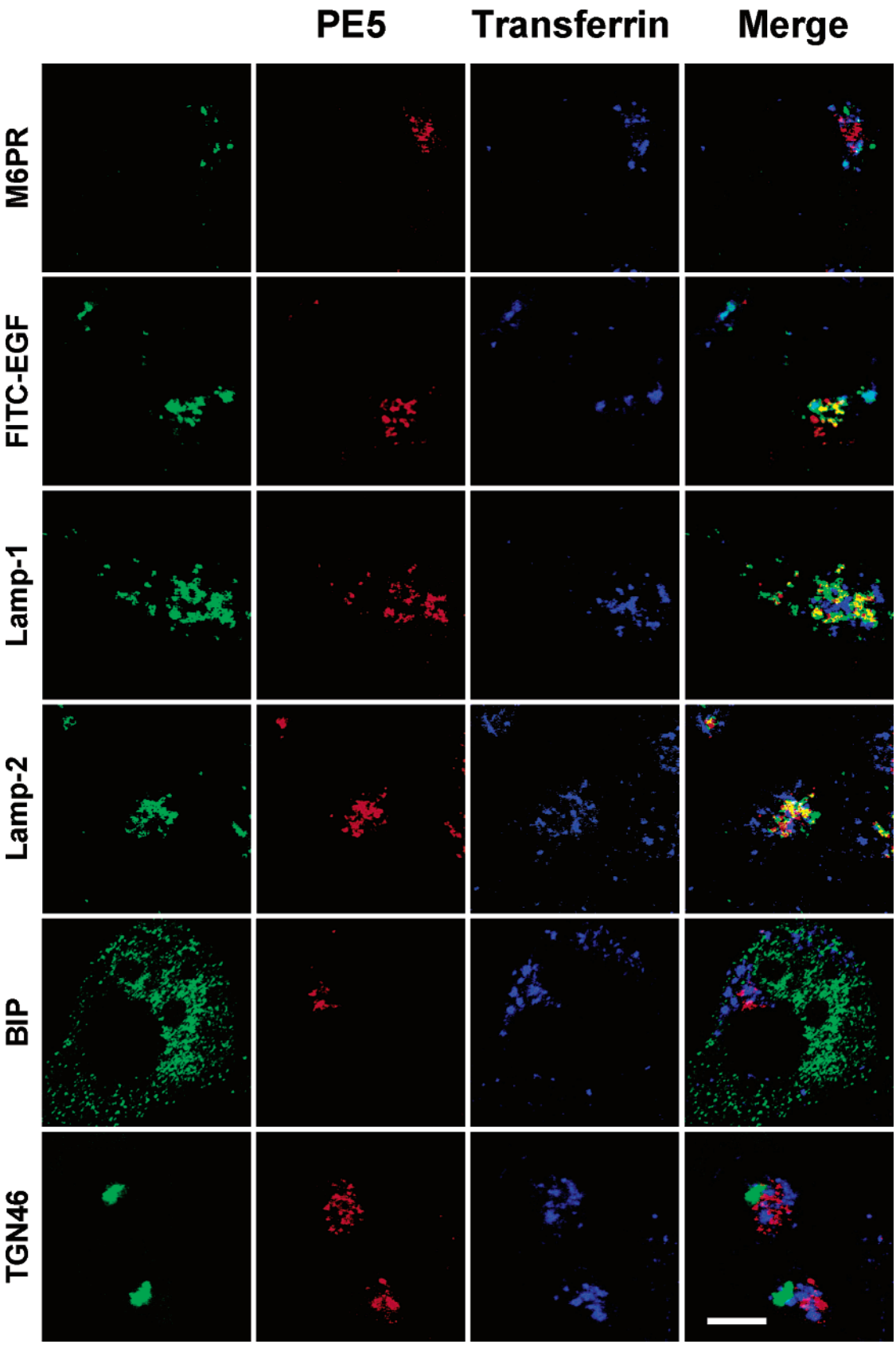

FIGURE 5: Internalization of fluorescent PE5 by A431 cells. A431 cells were labeled with Alexa Fluor 594-PE5 (red) for 24 h. Cy5-labeled transferrin (blue) was present for the last 45 min to label early endosomes. When indicated, fluorescein-labeled EGF (green), a tracer which is addressed to lysosomes, was added for the last hour of labeling. Cells were then processed for immunodetection (green) of lysosomal protein Lamp-1 or Lamp-2, the late endosome marker M6PR, the ER lumen chaperone BIP, or the *trans*-Golgi network marker TGN46. After being mounted, cells were observed under a confocal microscope. Representative medial optical sections of one to four cells are shown. The scale bar is 10 μm long. PE5 colocalized only with the lysosome markers, as indicated by yellow pixels (red and green) on the merged image.

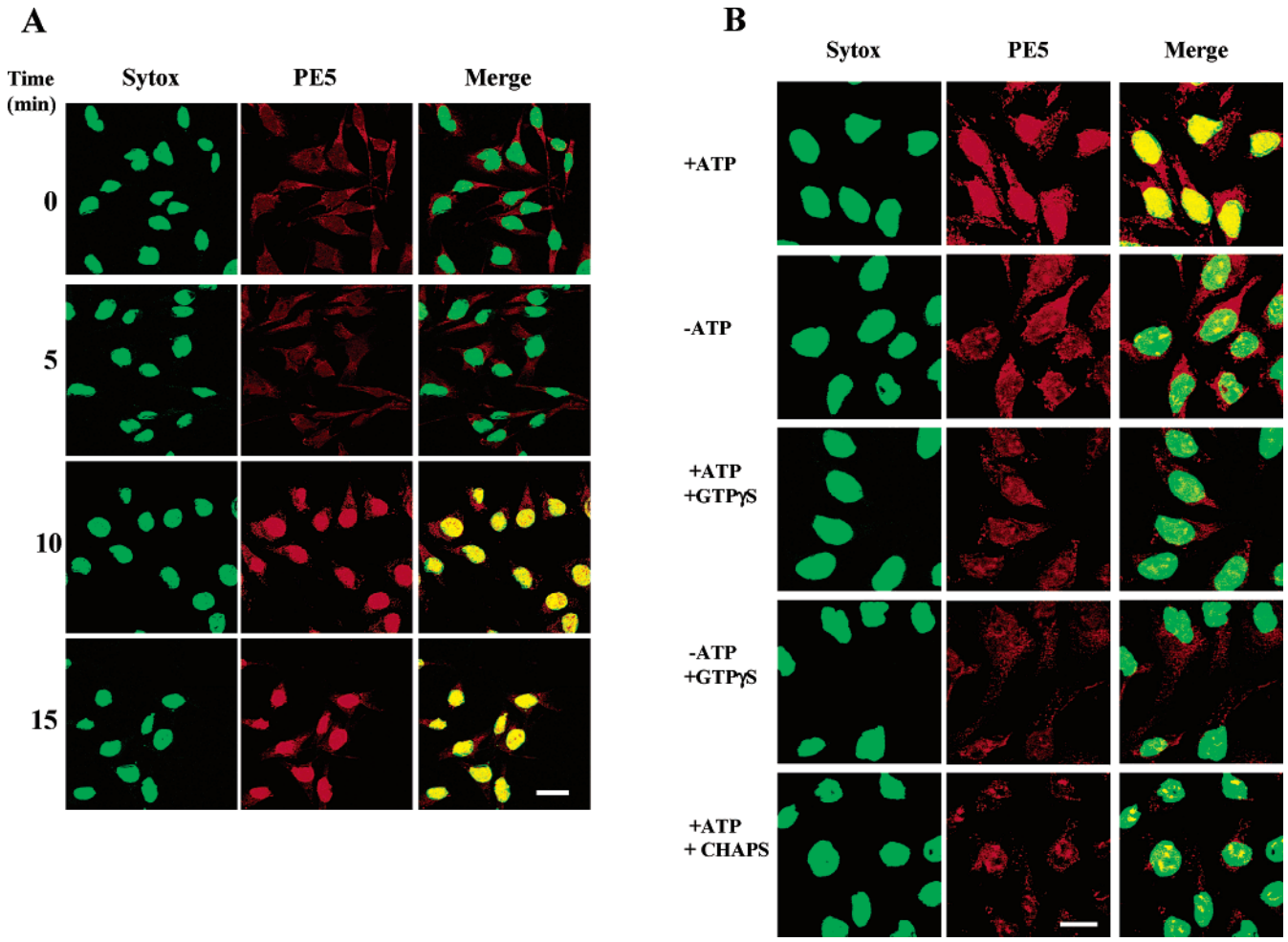

FIGURE 6: Characterization of PE5 nuclear import. HeLa cells were permeabilized with digitonin before the addition of cytosol and fluorescent PE5 (red). Import reactions were performed at 30 °C, before fixation and nuclei labeling with Sytox green (green), a DNA-binding dye. Cells were then mounted for viewing under a confocal microscope, and medial optical sections were recorded. (A) Import kinetics. Import reactions were performed in the presence of an ATP regenerating system and for the indicated period of time. The scale bar is 30 μm long. (B) Mechanism of PE5 nuclear accumulation. Import reactions were performed for 12 min at 30 °C, in the presence of an ATP regenerating system (+ATP), an ATP depleting system (−ATP), GTPγS, or a permeabilization of the nuclear envelope using CHAPS, as indicated. The scale bar is 20 μm long. Nuclear PE5 appears yellow in the merged image.

esized that, in PE5, the introduced triplet, possibly with the help of the pre-existing one, could act as an NLS.

The fact that PE5 could not be seen in the nucleus upon uptake does not necessarily mean that it is not directed to this structure; it may simply be that the number of molecules transported there is below the confocal microscope detection threshold. For instance, when monitoring uptake of exogenous HIV-1 Tat, which is known to be efficiently transported to the nucleus once it enters the cytosol (*38*), we never observed it in the nucleus (Vendeville, A., et al., manuscript submitted for publication). We therefore used digitonin-permeabilized cells in a conventional nuclear import assay to enable PE5 to be directly introduced into the cytosol and examine whether it was targeted to the nucleus. Digitonin is known to effectively permeabilize the plasma membrane but not the nuclear envelope (*28*, *29*).

In the presence of an ATP regenerating system, PE5 was efficiently imported into the nucleus, which took ~10 min at 30 °C (Figure 6A). PE5 was not imported in the presence of an ATP depleting system or of GTPγS, a nonhydrolyzable analogue of GTP (Figure 6B). Both these treatments result in an inhibition of Ran-mediated nuclear import (*39*). When NLS−BSA−fluorescein nuclear import was examined, it was found to follow the same kinetics (data not shown) and was similarly inhibited by ATP depletion with or without GTPγS (Figure 7A). We concluded that PE5 is targeted to the nucleus using the conventional NLS-mediated import machinery that requires Ran-GTPase activity. Hence, the Arg triplet introduced at positions 89−91 in PE5 enables efficient nuclear targeting.

Neither the parental variant PM5 nor 70 kDa dextran was imported into the nucleus, which confirmed the specificity of the transport and the integrity of the nuclear membrane (Figure 7B,C). At the onset of import (data not shown), and in the presence of CHAPS which permeabilizes the nuclear envelope and allows protein diffusion between the cytoplasm and the nucleoplasm, PE5 was observed to be concentrated in discrete intranuclear foci reminiscent of the nucleolus (Figure 6B). This structure was identified using Ki-67 localization by immunofluorescence (Figure 8).

Ultrastructural characterization of the nucleolus defined three distinct concentric substructures, each containing specific markers (or a combination of them), which are thought to be associated with distinct functions. The fibrillar

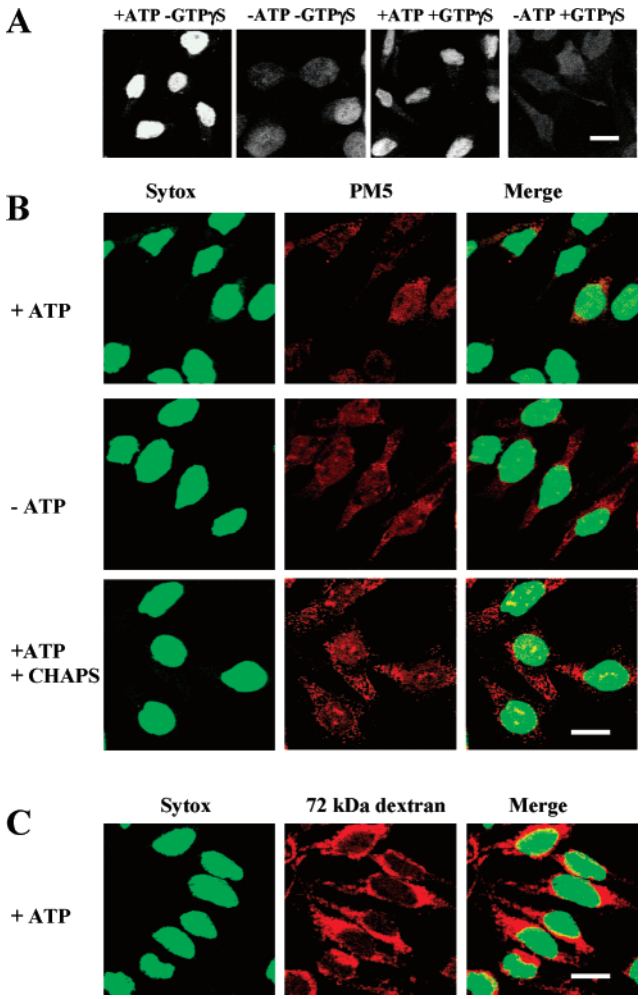

FIGURE 7: Controls for PE5 NLS-mediated nuclear import. Import reactions were performed for 12 min at 30 °C in the presence of cytosol, an ATP regenerating system. and (A) fluorescein−BSA−NLS (green), (B) fluorescent PM5 (red), or (C) 72 kDa rhodamine-bound dextran (red). Scale bars are 30 μm long. When indicated, the cell nucleus was labeled with Sytox green. The yellow color indicates markers overlapping. Only PM5 and dextran enter the nucleus when the nuclear envelope is permeabilized with CHAPS.

center is surrounded by the dense fibrillar component where the Ki-67 nucleolar marker is located, and the granular component forms the outer layer of the structure. Pre-rRNA processing is thought to occur in a radial manner in the nucleolus. Active rRNA transcription by RNA polymerase I takes place within the fibrillar center, while the granular component is the site of maturation and storage of preribosomal particles (*30*). The fact that PE5 shows an internal localization compared to Ki-67 within the nucleolus (Figure 8) indicates that the ribonuclease is present within the fibrillar center, and may be to some extent within the dense fibrillar component since some overlap between PE5 and Ki-67 labeling was observed. Hence, this result suggests that PE5 interacts with rRNA before packaging and not with preribosomal particles which are present outside the zone containing Ki-67 (*30*).

In the presence of CHAPS, both PE5 (Figure 6B) and the parent variant PM5 (Figure 7B) were observed within nucleoli, indicating that interaction with these structures merely results from the affinity of HP-RNase for rRNA and is not the consequence of the changes introduced into PE5.

DISCUSSION

Mutant Design. Several works have suggested that pancreatic-type ribonucleases with increased K_i values for the RI become cytotoxic. In the case of RNase A, a single amino acid change was enough to endow this enzyme with cytotoxic properties (*10*). The same approach was used with the HP-RNase homologue (sequence 70% identical with that of RNase A), although multiple substitutions were required to obtain a similar effect (*8*). We presented a molecular model, generated using a molecular dynamics approach, of the interaction of an HP-RNase variant with the RI (*31*). The same regions were also important for the interaction of the RI with RNase A (*32*). To preclude HP-RNase−RI interaction, we avoided mutating residues that might be important for catalysis. An exception was made with variants PE3I2 and PI5, which both carry the Lys66Arg substitution. Although Lys66 has been described as belonging to a p_0 noncatalytic phosphate binding subsite (*40*) and as playing a role in stabilizing the transition state, its conservative substitution with an Arg did not drastically affect the catalytic efficiency of the enzyme (Table 2). All variants presented a catalytic activity clearly higher than that of Onconase.

Mutants with the RGD insertion were designed to potentially increase cell binding and/or internalization efficiency (*18*), as this is thought to convert a noncytotoxic ribonuclease into a toxic one (*1*). Nevertheless, the RGD motif must be accessible at the protein surface to enable integrin binding. We introduced the RGD motif within different scaffolds, either within a disulfide-constrained loop ($\beta2\beta3$) or within flexible loops ($\alpha2\beta1$ and $\beta4\beta5$) (see Table 1 and Figure 1). None of these variants was more efficiently bound or internalized by cells than the control PM5 ribonuclease (Figure 4). In fact, when the RGD tripeptide is inserted into loops $\alpha2\beta1$ and $\beta2\beta3$ of PE3, to render PE3I1 and PE3I2, respectively, its cytotoxic activity is suppressed despite having an increased K_i for the RI (Table 2)

Variants PE5 and PE3 were designed to diminish the strength of the RNase−RI interaction with the aim of endowing them with cytotoxic properties. This turned out to be true in the case of PE3, confirming that RI evasion can convert an innocuous ribonuclease into a toxic molecule (*8*, *10*, *12*). In the case of PE5, the two Arg residues introduced at positions 89 and 90 were supposed to promote steric hindrance with a cluster of three Trp residues from the RI. These changes only slightly decreased the affinity for the RI (Figure 2). These data are consistent with the report that HP-RNase point mutations G89R and S90R only marginally reduced the affinity for RI (*12*).

Variant Stability. Enzyme stability has been reported to be an important parameter in the design of cytotoxic ribonucleases. Indeed, a positive correlation between thermostability and cytotoxicity has been described for RNase A (*7*, *10*). The variants described in this work have a lower thermal stability than the parental PM5, indicating that the mutations that were introduced were generally destabilizing. Nevertheless, as could be anticipated from the mutant design (e.g., the fact that the mutations were introduced within loops), and according to circular dichroism data, the secondary structure of the parent molecule was not affected in any of the variants. Interestingly, the cytotoxic variant PE5 was the second most unstable [from thermal denaturation data

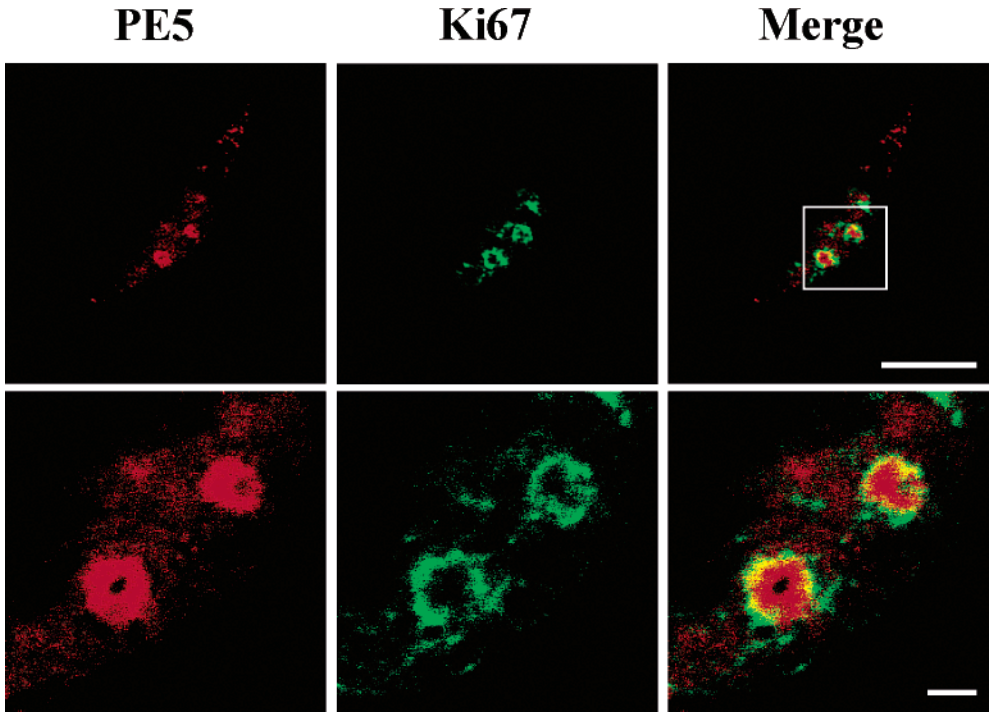

FIGURE 8: PE5 intranucleolar localization. HeLa cells were permeabilized with digitonin. Nuclear import reactions were performed for 7 min at 30 °C, using fluorescent PE5 (red) as a substrate, in the presence of cytosol and of an ATP regenerating system. Cells were then washed, fixed, and processed for immunostaining of Ki-67 (green). Medial optical sections were obtained with a confocal microscope. The boxed region in the top panel (scale bar is 20 μm) was rescanned and displayed with a higher magnification in the bottom panel (scale bar is 2 μm). In the merged image, areas of colocalization are yellow.

(Table 2)] and less compact [from thermolysin digestion sensitivity (data not shown)]. Hence, thermostability is not a strict requirement for ribonuclease cytotoxicity.

Variant Internalization. When endocytosis efficiency was assessed using a conventional ^{125}I-labeled tracer uptake assay, none of the variants was significantly endocytosed compared to Onconase (Figure 4). Nevertheless, when a more sensitive confocal microscopic approach was used, both PE5 (Figure 5) and PM5 (not shown) could be observed intracellularly. Their intracellular visualization nevertheless required uptake for 24 h. At that time, they were found within lysosomes, and no evidence for retrograde transport to elements of the Golgi apparatus or the ER was found (Figure 5).

These data confirm previous results indicating that translocation from some elements of the endocytic pathway is what gives ribonucleases access to the cytosol (*4*), and indicates that ribonucleases are not subjected to retrograde transport toward the ER or the Golgi apparatus, as is the case for some bacterial toxins (*41*).

No difference in intracellular routing was found among the two variants that were studied (PM5 and PE5). Since endocytosis of fluorescent tracers was not significantly inhibited by an excess of unlabeled PM5 or PE5 (data not shown), we concluded that they entered cells essentially via fluid-phase uptake. This result is consistent with the lysosomal destination of endocytosed ribonucleases (Figure 5), and their low endocytosis efficiency compared to Onconase (Figure 4), for which a cellular receptor is postulated (*11*). It therefore seems that the specific ability of Onconase to be efficiently endocytosed is partly responsible for its toxicity being higher than those of our variants.

Cytotoxicity and Nuclear Import. Variants exhibiting a K_i for the RI in the nanomolar range were good candidates for being cytotoxic (*8*, *10*). Surprisingly, only PE3 and PE5 were toxic to cells, the latter despite being the least resistant to the RI. While this might indicate that ribonuclease cytotoxicity does not necessarily require RI avoidance, we showed that the nuclear import triggered by the changes introduced in PE5 enabled it to bypass the cytosolic RI.

It should be mentioned that the altered loop containing the Arg triplet recognized by the NLS-dependent nuclear import machinery is also a site for RI binding. Hence, either the RI or importin α can bind to PE5 but, very likely, not both at the same time. Consequently, it is unlikely that PE5 drags the cytosolic RI along with it into the nucleus.

The presence of the cytosolic RI clearly did not prevent PE5 nuclear accumulation (compare Figure 6 for PE5 to Figure 7A for fluorescein−BSA−NLS). We believe that this may be because importin α has an affinity for PE5 that makes it strong enough to compete with the RI for PE5 binding. In addition, since PE5 weakly evades the RI (Figure 2), there will be minute amounts of cytosolic PE5 that are not RI-bound and will therefore be available for nuclear import. The resulting drop in the level of free PE5 molecules in the cytosol will displace the RI−PE5 complexes toward dissociation, and progressively, PE5 will accumulate within the nucleus.

On the basis of these results, we cannot precisely define the NLS sequence present in PE5. Since the parent variant PM5 already has an Arg triplet (residues 31−33) within a surface-exposed loop and it is not targeted to the nucleus, it is clear that the RRR motif is not by itself an NLS sequence. Thus, residues neighboring the Arg triplet of residues 89−91 (sequentially adjacent or spatially close) might also be involved in the recognition of PE5 by the nuclear import machinery.

Concluding Remarks. The introduction of two Arg residues before pre-existing Arg91 in PM5 generated the PE5 variant which, compared to the other variants, was the most cytotoxic but is neither the most stable nor the most resistant to the RI and which is not more efficiently taken up by cells. Moreover, the net charge of PE5 is the same as that of nontoxic wild-type HP-RNase (PM9 in Table 2). PE5 cytotoxicity therefore did not result from cationization either. Its sole specificities are its nuclear and/or nucleolar targeting and its toxicity. We conclude that targeting an HP-RNase variant to the nucleus and/or nucleolus results in cytotoxicity. In addition, this work indicates that RI evasion is not essential to endow a pancreatic ribonuclease with cytotoxic properties.

Ribonucleases have much potential as chemotherapeutics. Among the members of the ribonuclease superfamily, Onconase is the paradigm, since it is undergoing phase II/III human clinical trials for the treatment of different types of cancer (*2*). In this paper, we showed that directing a ribonuclease to the nucleus is a new strategy for preparing cytotoxic ribonucleases. The variant targeted at the nucleus, PE5, is less cytotoxic than Onconase. Nevertheless, being a protein of human origin, it should be less immunogenic and have a lower renal toxicity than Onconase, and it might, therefore, warrant clinical assessment.

ACKNOWLEDGMENT

We are very grateful to Urs Greber (Zurich, Switzerland), Ronald Raines (Madison, WI), and Henri Rochefort (Montpellier, France) for providing us with fluorescein−BSA−NLS, the Onconase gene, and the antibody against M6PR, respectively.

REFERENCES

1. Rybak, S. M., and Newton, D. L. (1999) *Exp. Cell Res. 253*, 325−335.
2. Saxena, S. K., Sirdeshmukh, R., Ardelt, W., Mikulski, S. M., Shogen, K., and Youle, R. J. (2002) *J. Biol. Chem. 277*, 15142−15146.
3. Vasandani, V. M., Burris, J. A., and Sung, C. (1999) *Cancer Chemother. Pharmacol. 44*, 164−169.
4. Haigis, M. C., and Raines, R. T. (2003) *J. Cell Sci. 116*, 313−324.
5. Leland, P. A., and Raines, R. T. (2001) *Chem. Biol. 8*, 405−413.
6. Notomista, E., Catanzano, F., Graziano, G., Di Gaetano, S., Barone, G., and Di Donato, A. (2001) *Biochemistry 40*, 9097−9103.
7. Klink, T. A., and Raines, R. T. (2000) *J. Biol. Chem. 275*, 17463−17467.
8. Leland, P. A., Staniszewski, K. E., Kim, B. M., and Raines, R. T. (2001) *J. Biol. Chem. 276*, 43095−43102.
9. Haigis, M. C., Kurten, E. L., and Raines, R. T. (2003) *Nucleic Acids Res. 31*, 1024−1032.
10. Leland, P. A., Schultz, L. W., Kim, B. M., and Raines, R. T. (1998) *Proc. Natl. Acad. Sci. U.S.A. 95*, 10407−10412.
11. Wu, Y., Mikulski, S. M., Ardelt, W., Rybak, S. M., and Youle, R. J. (1993) *J. Biol. Chem. 268*, 10686−10693.
12. Gaur, D., Swaminathan, S., and Batra, J. K. (2001) *J. Biol. Chem. 276*, 24978−24984.
13. Piccoli, R., Di Gaetano, S., De Lorenzo, C., Grauso, M., Monaco, C., Spalletti-Cernia, D., Laccetti, P., Cinatl, J., Matousek, J., and D'Alessio, G. (1999) *Proc. Natl. Acad. Sci. U.S.A. 96*, 7768−7773.
14. Roth, J. S., and Juster, H. (1972) *Biochim. Biophys. Acta 287*, 474−476.
15. Leonidas, D. D., Shapiro, R., Subbarao, G. V., Russo, A., and Acharya, K. R. (2002) *Biochemistry 41*, 2552−2562.
16. Lixin, R., Efthymiadis, A., Henderson, B., and Jans, D. A. (2001) *Biochem. Biophys. Res. Commun. 284*, 185−193.
17. Xu, Z. P., Tsuji, T., Riordan, J. F., and Hu, G. F. (2002) *Biochem. Biophys. Res. Commun. 294*, 287−292.
18. Rouslahti, E. (1996) *Annu. Rev. Cell Dev. Biol. 12*, 697−715.
19. Juncosa-Ginesta, M., Pons, J., Planas, A., and Querol, E. (1994) *BioTechniques 16*, 820−823.
20. Ribo, M., Benito, A., Canals, A., Nogues, M. V., Cuchillo, C. M., and Vilanova, M. (2001) *Methods Enzymol. 341*, 221−234.
21. Gill, S. C., and von Hippel, P. H. (1989) *Anal. Biochem. 182*, 319−326.
22. Stone, S. R., and Hofsteenge, J. (1986) *Biochemistry 25*, 4622−4628.
23. Boix, E., Wu, Y., Vasandani, V. M., Saxena, S. K., Ardelt, W., Ladner, J., and Youle, R. J. (1996) *J. Mol. Biol. 257*, 992−1007.
24. Leatherbarrow, R. J. (1987) *ENZFITTER*, Elsevier Biosoft, Cambridge, U.K.
25. Torrent, J., Connelly, J. P., Coll, M. G., Ribo, M., Lange, R., and Vilanova, M. (1999) *Biochemistry 38*, 15952−15961.
26. Alami, M., Taupiac, M. P., Reggio, H., Bienvenue, A., and Beaumelle, B. (1998) *Mol. Biol. Cell 9*, 387−402.
27. Beaumelle, B., Taupiac, M. P., Lord, J. M., and Roberts, L. M. (1997) *J. Biol. Chem. 272*, 22097−22102.
28. Kehlenbach, R. H., Dickmanns, A., and Gerace, L. (1998) *J. Cell Biol. 141*, 863−874.
29. Moore, M. S., and Blobel, G. (1992) *Cell 69*, 939−950.
30. Kill, I. R. (1996) *J. Cell Sci. 109*, 1253−1263.
31. Pous, J., Canals, A., Terzyan, S. S., Guasch, A., Benito, A., Ribo, M., Vilanova, M., and Coll, M. (2000) *J. Mol. Biol. 303*, 49−60.
32. Kobe, B., and Deisenhofer, J. (1996) *J. Mol. Biol. 264*, 1028−1043.
33. Zanetti, M., Filaci, G., Lee, R. H., del Guercio, P., Rossi, F., Bacchetta, R., Stevenson, F., Barnaba, V., and Billetta, R. (1993) *EMBO J. 12*, 4375−4384.
34. Pasqualini, R., Koivunen, E., and Ruoslahti, E. (1997) *Nat. Biotechnol. 15*, 542−546.
35. Morrison, J. F., and Walsh, C. T. (1988) *Adv. Enzymol. Relat. Areas Mol. Biol. 61*, 201−301.
36. Futami, J., Maeda, T., Kitazoe, M., Nukui, E., Tada, H., Seno, M., Kosaka, M., and Yamada, H. (2001) *Biochemistry 40*, 7518−7524.
37. Gruenberg, J. (2001) *Nat. Rev. Mol. Cell Biol. 2*, 721−730.
38. Truant, R., and Cullen, B. R. (1999) *Mol. Cell. Biol. 19*, 1210−1217.
39. Schwoebel, E. D., Ho, T. H., and Moore, M. S. (2002) *J. Cell Biol. 157*, 963−974.
40. Nogues, M. V., Moussaoui, M., Boix, E., Vilanova, M., Ribo, M., and Cuchillo, C. M. (1998) *Cell. Mol. Life Sci. 54*, 766−774.
41. Johannes, L., and Lamaze, C. (2002) *Traffic 3*, 443−451.
42. Koradi, R., Billeter, M., and Wuthrich, K. (1996) *J. Mol. Graphics 14*, 51−55.

BI035729+